# **Acoustic Holography with Crossed Linear Arrays**

Abstract: This paper is an analysis of how acoustic (or microwave) holography can be applied to large masses, such as natural bodies of water or the earth, by means of a linear array of microphones and by scanning with one or more transmitters to produce holographic phase shifts. This type of hologram, in which the phased array has a conical antenna pattern, is shown to be superior to the area hologram for computing images in the near field. Computer simulations are given of virtual holograms and image reconstructions for specular and diffuse reflectors; simulations are also made for the case of pulse holography, which yields geniune three-dimensional images with reduced highlight distortions.

## Introduction

When acoustic (or microwave) holography is extended to uncontrolled media outside the laboratory, such as natural bodies of water, two unique problems arise. The first problem is the question of how to constrain the spatial extent of the hologram plane, which is made large as a result of the long wavelengths that must be used. The second problem concerns the need to retain the range-gating features that are so valuable in sonar or radar, but which to date have not been integrated into the concept of holography. By means of computer simulations we have demonstrated that both problems can be solved in a practical way. The solution to the first problem, i.e., the optimum means to reduce the spatial extent and number of transducers required to generate a hologram, is described in an earlier paper. In this paper we briefly review the scheme, which employs crossed linear arrays, and then proceed to describe our simulations of virtual holograms and image reconstructions based on very brief pulses. We also describe some features that make the technique particularly suitable for image reconstruction by computer.

#### Review of crossed linear arrays

In natural bodies of water, the earth or other media not amenable to control by the experimenter, the main impediments to acoustic holography are the attenuation of the signal and the refractive disturbances that scramble the phase of the signal. The only effective countermeasure is to employ wavelengths much longer than those customarily used in the laboratory. The lower frequencies propagate much farther and the long wavelengths provide

greater tolerance to refractive disturbances. Unfortunately, the use of long wavelengths carries with it the requirement for a large hologram surface, i.e., for a large effective aperture, since aperture varies in proportion to wavelength for constant resolving power. The only reasonable way to cover a large effective aperture is by deploying an array of microphones over the hologram surface or by scanning the surface with one or a group of microphones.

Figures 1, 2, and 3 illustrate the new concept as a succession of modifications to conventional acoustic holography. Figure 1(a) represents the impractical ideal in which a large array of microphones fills the hologram surface, and Fig. 1(b) represents the slow scan usually employed to synthesize the complete hologram.<sup>2</sup> Figure 2(a) shows a modification that is more nearly practical—a compromise in which the surface is synthesized by scanning a linear array sideways. Figure 2(b) is the same except that the roles of transmitter and receiver are switched, a reversal that Metherell and Spinak<sup>3</sup> demonstrated and proved valid.

Our contribution derives from the observation that the transducers (either transmitting or receiving) in a linear array can be stationary while the *other* single transducer scans perpendicular to the array and thereby generates the holographic phase shifts as in Fig. 3(a). The phase shifts are slightly different from those of a true hologram, but are equally valid for image reconstruction when processed properly. Figure 3(b) shows how the single transducer scan can be replaced by a second linear array, a final obvious modification that eliminates moving parts altogether. The transmitting elements emit pulses in sequence to simulate a scan, but are capable of higher scan velocity than the single, moving transducer.

The authors are with Tetra Tech, Incorporated, Pasadena, California 91107.

A set of  $N^2$  complex data points (amplitude and phase) constitutes a virtual square hologram with  $N \times N$  elements. The crossed linear arrays of Fig. 3(b) collect these data with only 2N transducers. The (n, m)th datum in this set results from listening to the mth transmitter with the nth receiver. We shall refer to the new type of hologram as a conic hologram, because the displacement of its fringes from those of a conventional hologram relates to the conical shape of the radiation pattern from a linear phased array. The conventional hologram will be called an area hologram to emphasize the property that either the transmitter or the receiver is extended in two dimensions by scanning, arraying or both. An essential feature of holography is that two dimensions are involved. Conic holography splits these, one to the transmitter and one to the receiver, while area holography gives both dimensions to one or the other. Unfortunately, experimental data are not yet available. However, there is every reason to expect that the distortions in real acoustic media will be identical to those already observed in acoustic area holography and in any other phase-sensitive acoustic technique. The important questions regarding the effect, or mostly noneffect, of the unorthodox geometry are answered by the simulation.

# Computer image reconstruction

In most of the papers given at the conference, "Holography and the Computer," the computer was employed to construct a hologram of a nonexistent object and an image was reconstructed in laser light. By contrast, the present paper discusses the prospects for taking an acoustic hologram of objects that do exist and reconstructing the image with the aid of the computer, eliminating the laser entirely. In Ref. 1 we showed that conic and area holography are equivalent in the far field up to the point where the Fresnel approximation fails. We now show that, even in the near field, conic holography is suitable for computer reconstruction, whereas area holography becomes prohibitively time consuming. This near-field computing advantage is a result of a convenient separation of variables peculiar to the conic geometry.

Figure 4 shows the geometry of crossed linear arrays superimposed on the geometry of a conventional area hologram. The object plane  $(\xi, \eta)$  is parallel to the hologram plane (x, y) at a distance R'. A typical reflecting point on the surface of an insonified object is denoted by  $P(\xi, \eta)$ . As drawn, the figure applies to reflection holography, although the principles are readily extended to transmission holography. For conic holography the two arrays lie along the x and y axes. The dashed lines between planes represent a typical round-trip propagation path from an element P(x, 0) in the transmitting array to an element P(0, y) in the receiving array. (Each dashed line is one element of the cone that would be generated

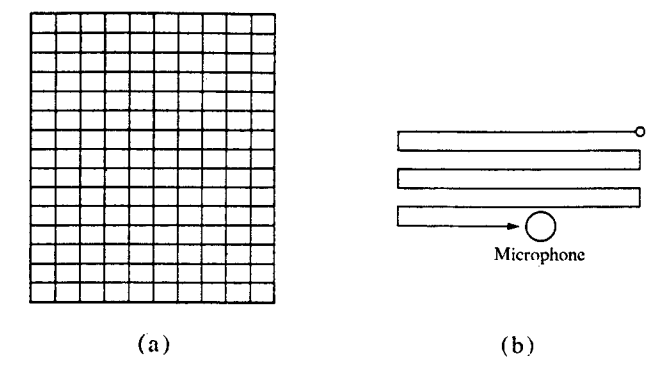


Figure 1 Impractical ideal in which (a) a large array of  $N^2$  microphones is usually replaced by (b) a raster scan by one microphone over the hologram plane.

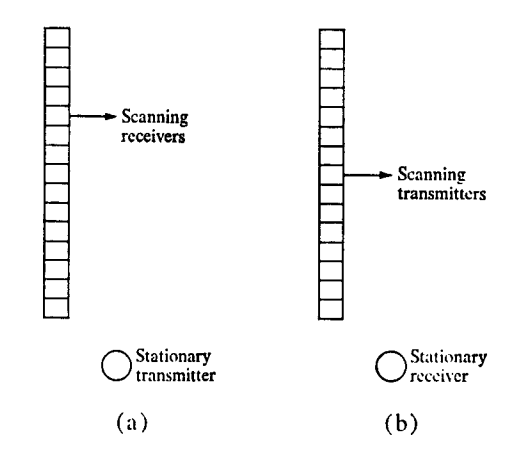


Figure 2 In one possible compromise a linear array can scan sideways and synthesize the hologram. (a) The receiver does the scanning; (b) the transmitter scans while the receiver is stationary.

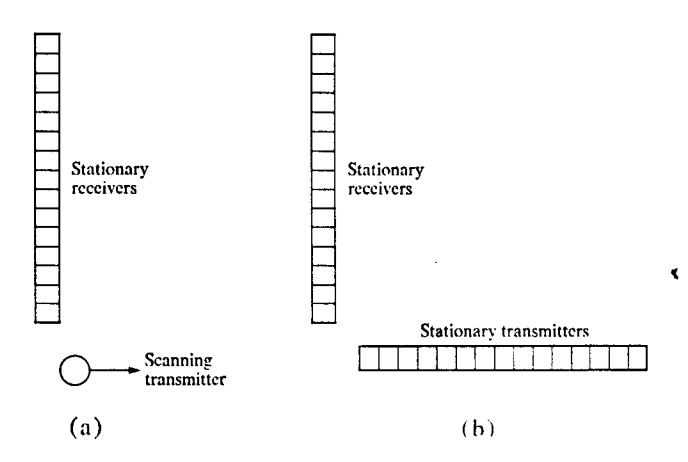


Figure 3 Conic holography generates holographic phase shifts by (a) leaving the linear array stationary and scanning the single transducer in a direction perpendicular to the array, or (b) using a second linear array to replace the linear scan. This provides a very fast scan without moving parts.

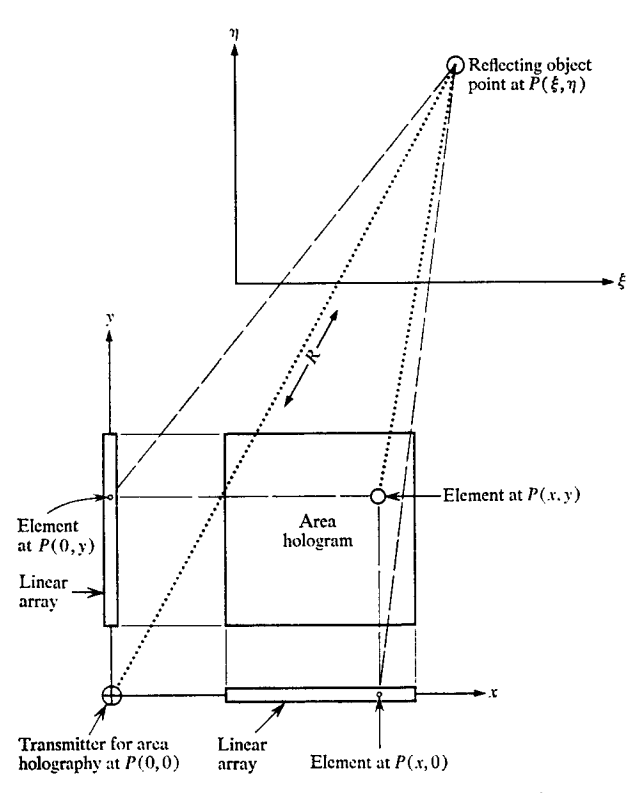


Figure 4 The geometry of crossed linear arrays is superposed on that of area holography to study the phase shifts of one relative to the other. The dashed round-trip propagation path is for conic holography, the dotted one for area holography. The end points of these paths in the hologram plane define a rectangle. The conic end points lie on one diagonal, the area holography end points on the other.  $\Delta = (\text{dashed z-way path}) - (\text{dotted z-way path}) \approx (xy\xi n)/R^3$ .

by rotating the line about its axis, x or y.) For area holography the transmitter is assumed to be at the origin and the extended receiver area fills part of the (x, y) plane. The dotted lines represent a typical round-trip propagation path between the transmitter at P(0, 0) and a receiver positioned at P(x, y).

Let R' be the distance between the two planes. Then the two propagation path lengths are, for area holography and conic holography, respectively,

$$r_a = [R'^2 + \xi^2 + \eta^2]^{\frac{1}{2}} + [R'^2 + (x - \xi)^2 + (y - \eta)^2]^{\frac{1}{2}},$$
(1a)

$$r_{\rm e} = [R'^2 + (x - \xi)^2 + \eta^2]^{\frac{1}{2}} + [R'^2 + \xi^2 + (y - \eta)^2]^{\frac{1}{2}}.$$
 (1b)

Let 
$$R^2 = R'^2 + \xi^2 + \eta^2$$
; then

$$r_{\rm a} = R + [R^2 + x(x - 2\xi) + y(y - 2\eta)]^{\frac{1}{2}},$$
 (2a)

$$r_c = [R^2 + x(x - 2\xi)]^{\frac{1}{2}} + [R^2 + y(y - 2\eta)]^{\frac{1}{2}}.$$
 (2b)

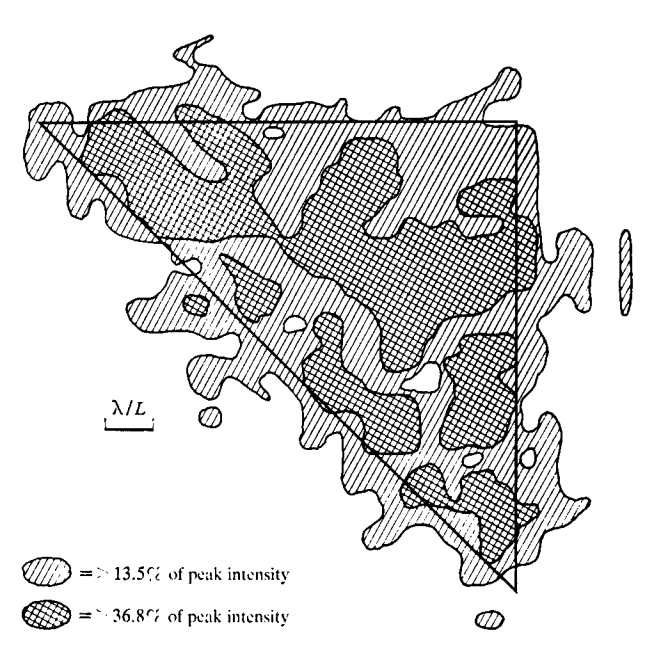


Figure 5 Computed image of a diffusely reflecting triangle. The image was obtained from a phase hologram simulating the output of a  $30 \times 30$  crossed array. Hatching and cross-hatching represent  $e^{-2}$  and  $e^{-1}$  of peak intensity. The random pattern is like the speckle pattern of a diffuse surface viewed in laser light.

The expansion of the square roots in the above equations to second order would give the Fresnel approximation, and one can readily show that in this approximation Eqs. (2a) and (2b) are identical. However, in the near field, evaluations of square roots could consume a prohibitive amount of computer time. Therefore we look for some means to store a table of square roots in advance within the computer memory and use this table repeatedly. With Eq. (2a) this scheme does not work well because the square root is a function of four variables, R, x,  $\xi$ and  $\eta$ . However, in Eq. (2b) the two square roots have the same form and can both be evaluated from a single table. Each of the square roots is a function of only three variables, so it becomes reasonable to tabulate the functions in advance when the variables do not take an excessively large number of different values. Obviously, the natural way to build up a three-dimensional image is to take spherical cuts through it (that is, let R = const.) and to plot image intensity in  $\xi$  and  $\eta$  for each of these cuts. In this way we repeatedly use a smaller table in which R is constant and x and  $\xi$  are the only variables; after each use, the table may be erased and replaced with a similar table for a different value of R.

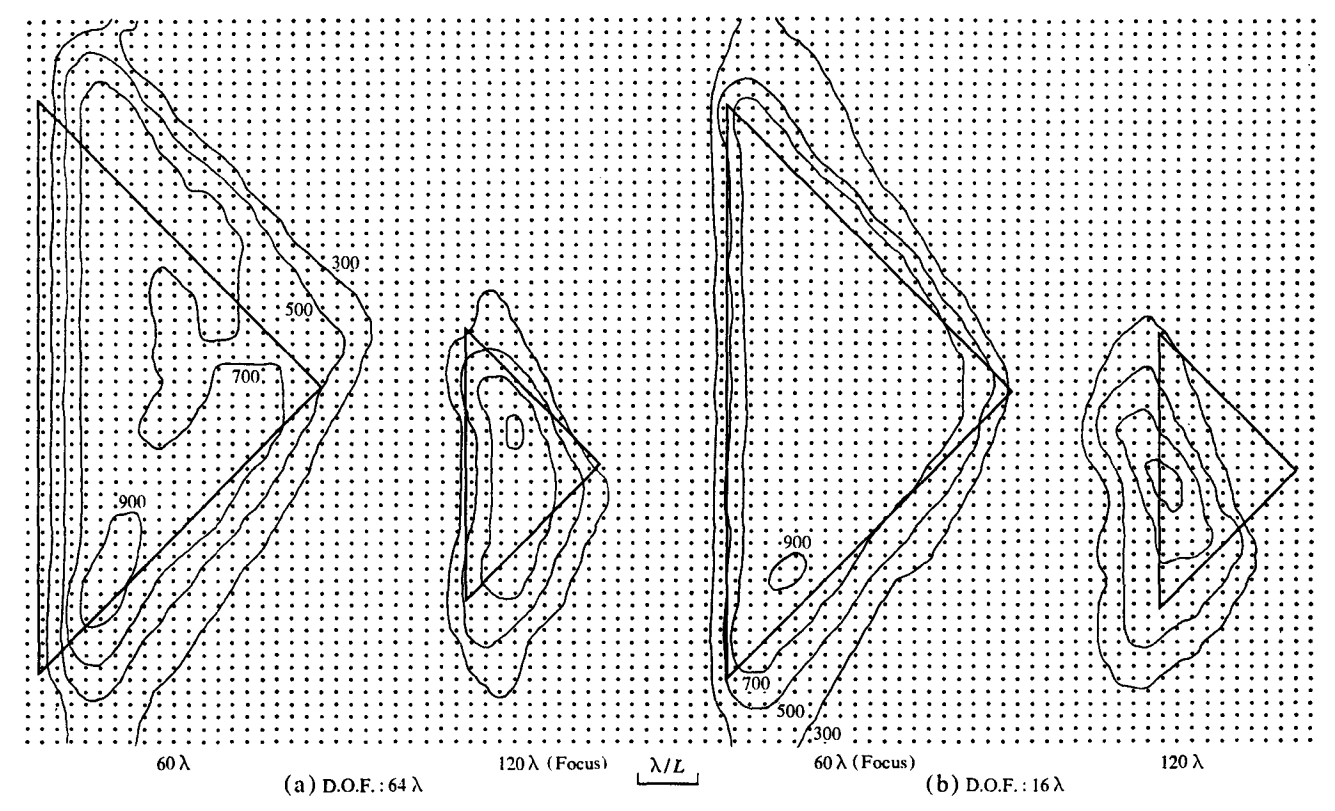


Figure 6 Computed images of two specular triangles; the images were obtained from the same phase hologram. (a) The triangle is in focus at a range of 120λ; (b) the triangle is in focus at 60λ. Range discrimination is marginal. Maximum intensity is 1000. D.O.F. is the nominal depth-of-field.

An IBM System/360 Model 44 has been employed to simulate complex-phase acoustic holograms generated by a 30-transmitter × 30-receiver crossed array. Figures 5 and 6 are intensity-contour maps of representative image reconstructions. Except for minor diffraction effects attributable to the rectangular mesh quantization, these images are indistinguishable from conventional holographic images. (For a detailed comparison, see Ref. 1.)

Figure 5 depicts the image resulting from a diffusely reflecting triangle. The reconstruction spans a small number of resolution elements to permit detailed rendition of the diffraction effects. The speckled appearance commonly associated with coherent imaging is clearly evident.

Figure 6 shows two computer reconstructions of a single acoustic phase-hologram. The hologram simulates two identical specularly reflecting right triangles at two ranges,  $60\lambda$  and  $120\lambda$ . The reconstructions are performed on the  $60\lambda$  and  $120\lambda$  focal surfaces. Although the  $30\lambda \times 30\lambda$  aperture produced some blurring of the out-of-focus triangle in each picture, the inherent lack of range discrimination is apparent.

#### Pulse holography

Acoustic holography at moderate frequencies enjoys an important advantage over optical holography; namely,

that acoustic signals intercepted by the receiving array can be amplified, directly recorded and coherently processed in a variety of ways. Moreover, acoustic holography need not be limited to a single frequency, but can employ wide-band signals of arbitrary waveform.<sup>5</sup>

A particularly useful waveform is a short, unbiased pulse. Such a pulse waveform is capable not only of angular object resolution but also of sharp range resolution, making possible truly three-dimensional reconstructions of actual object reflectivities. Two-dimensional holographic reconstructions from linear-array seismograms have already been exhibited. A pulse whose length in the propagating medium is  $\lambda$  can resolve objects separated either in range by  $\lambda/2$  or in angle by  $\lambda/L$ , where L is the hologram aperture.

This capability should be distinguished from that of conventional phase holography, in which three-dimensional object properties can be inferred only through selective focus or perspective/parallax, phenomena which are useful only at small focal ratios. Smooth, specularly reflecting objects are notoriously distorted under conventional holographic reconstruction since the main features are always specular highlights, that is, images of the transmitter, which dominate every reconstruction regardless of the focal plane. The simulations presented in

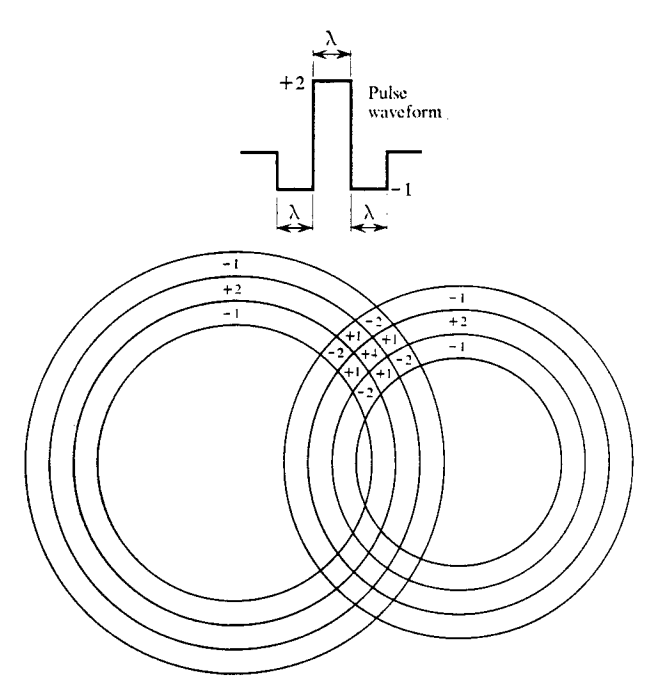


Figure 7 Idealized pulse hologram of two reflecting points at a single instant, for the pulse waveform shown inset. The numbers represent the instantaneous time derivative of received amplitude as a function of position x, y in the hologram plane. The smaller size of the right-hand zones indicates that the right-hand point is farther from the array.

the next section indicate that specular highlights are quite effectively tamed by the range discrimination of pulse holography.

## · Pulse holograms

A conventional acoustic hologram consists of a recorded complex amplitude H(x, y) for each point (x, y) on the hologram plane, where H(x, y) represents the steady-state interference pattern produced by the object in the field of a cw transmitter. In wide-band pulse holography phase is supplanted by a more general time-dependence: the hologram at each point (x, y) consists of a complete time record of reflected acoustic amplitude G(x, y, t). If f(t) is the transmitted amplitude waveform (at unit distance), and if  $s_1, s_2$  are the distances between a reflecting point p and the transmitter and receiver, respectively, then

$$G(x, y, t) = \sum_{p} \frac{\rho(p)}{s_1 s_2} f\left(t - \frac{1}{c} s_1 - \frac{1}{c} s_2\right), \qquad (3)$$

where  $\rho(p)$  is the effective density of reflectors, and c is the velocity of sound. An image of  $\rho(p)$  is reconstructed by time-reversed "playback" of the time-differentiated hologram,<sup>7</sup>

$$I(p) = \sum_{x,y} \frac{1}{s_1 s_2} G'\left(x, y, \frac{1}{c} s_1 + \frac{1}{c} s_2\right), \tag{4}$$

and displayed as an intensity  $I^2$ . The holographic geometry is only implicit in the above equations. In the conventional geometry the propagation distances depend on the point coordinates  $(\xi, \eta, R')$  and hologram coordinates x, y through

$$s_1 = s_1(\xi, \eta, R')$$
 and

$$s_2 = s_2(x, y, \xi, \eta, R'),$$

while in conic holography the dependency is through the convenient separated form

$$s_1 = s(x, \xi, R)$$
 and

$$s_2 = s(y, \eta, R),$$

as discussed earlier. Conic coordinates are vastly simpler for digital reconstruction and simulation, but are somewhat harder to visualize than the conventional geometry. For purposes of discussion, the distinction is unimportant since the two geometries result in topologically identical holograms.

Figure 7 shows schematically a pulse hologram of two reflecting points. The illustration represents the recorded, time-differentiated amplitudes in the hologram plane (x, y)at a single instant of time t. It should be visualized as the intersection of the hologram plane with expanding spherical wavefronts originating at the points at earlier times of reflection. The unbiased triple pulse (-1, +2,-1), used to represent the time derivative of a bipolar transmitted pulse, appears as concentric rings, expanding in the (x, y) plane as t increases; these rings are essentially the familiar Fresnel zones with time-dependence restored. Figure 8 is the corresponding digital simulation. The rectangular distortion of the zones is a result of digital quantization in space and time. Note how the range difference between the two points is recorded as relative time delay on the hologram.

# • Reconstructions

A pulse whose time derivative has the form shown in Fig. 7, with  $\lambda=1.0$ , has been used in the synthesis of several holograms comprising  $27\times27$  array sites. Figure 9 shows the geometry of two simulations for which results are presented. The object field subtends  $\pm30^{\circ}$  square and spans ranges of 15.0 to 18.75. The transducer spacing is 1.0; hence the array aperture is 27.0. The low focal ratio of 0.6 presents no computing problems, thanks to the crossed-linear-array conic geometry adopted for the simulation.

The reconstructions are presented in range increments of 0.25 and lateral (column): increments of 0.6 at mid-

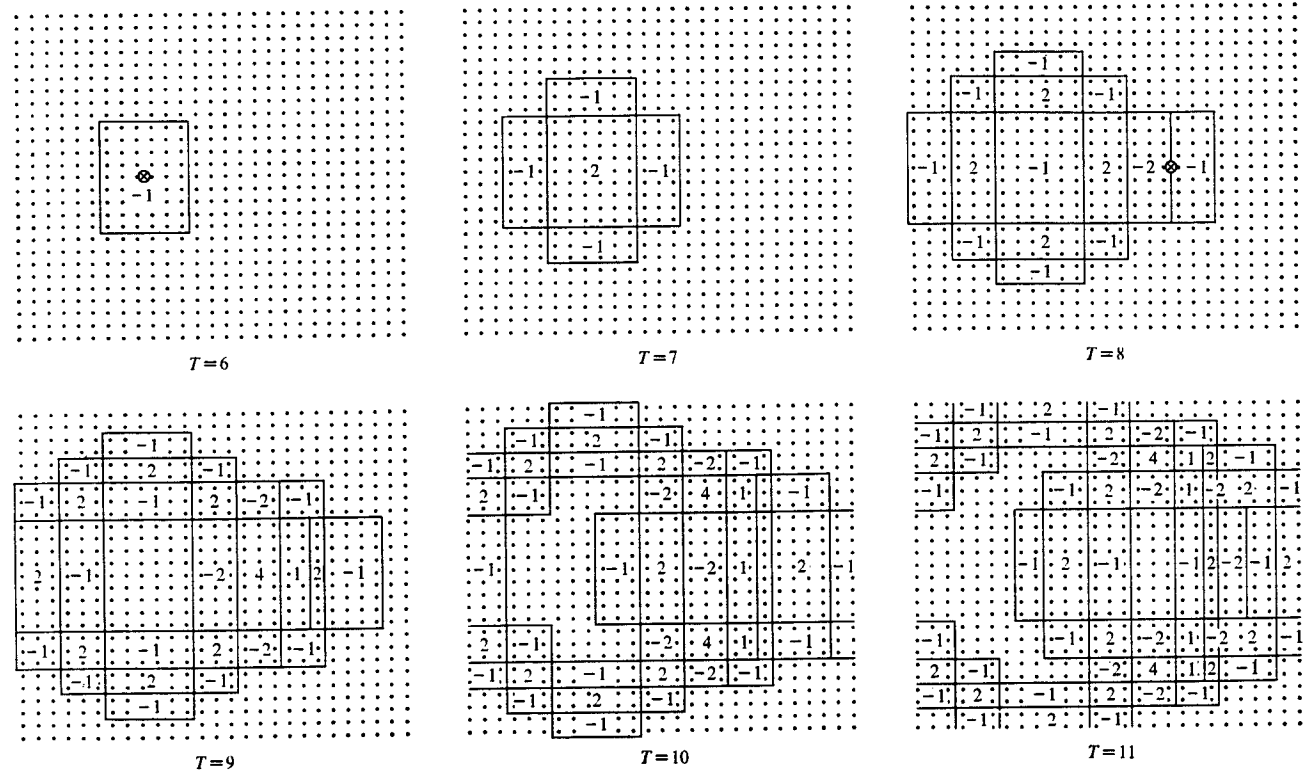
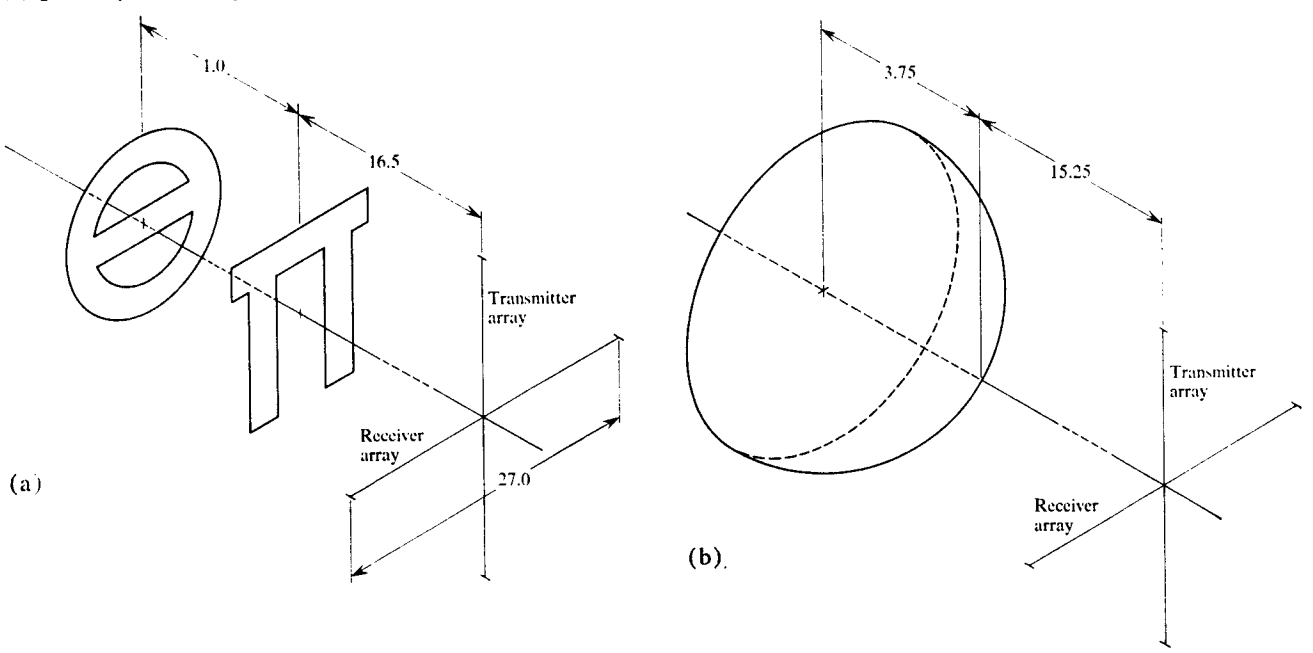


Figure 8 Digital simulation of a pulse hologram for two reflecting points. Ranges to the left- and right-hand points are 16.5 and 17.5, respectively. Instantaneous time-differentiated amplitudes are shown as a function of array coordinates x, y for integer times T=6 to T=11. Sound propagation speed c is taken to be unity.

Figure 9 Schematic depiction of array-object geometry for the simulations presented in Figs. 10-12. (a) Geometry for II and  $\Theta$ ; (b) geometry for hemisphere.



SEPTEMBER 1970 ACOUSTIC HOLOGRAPHY

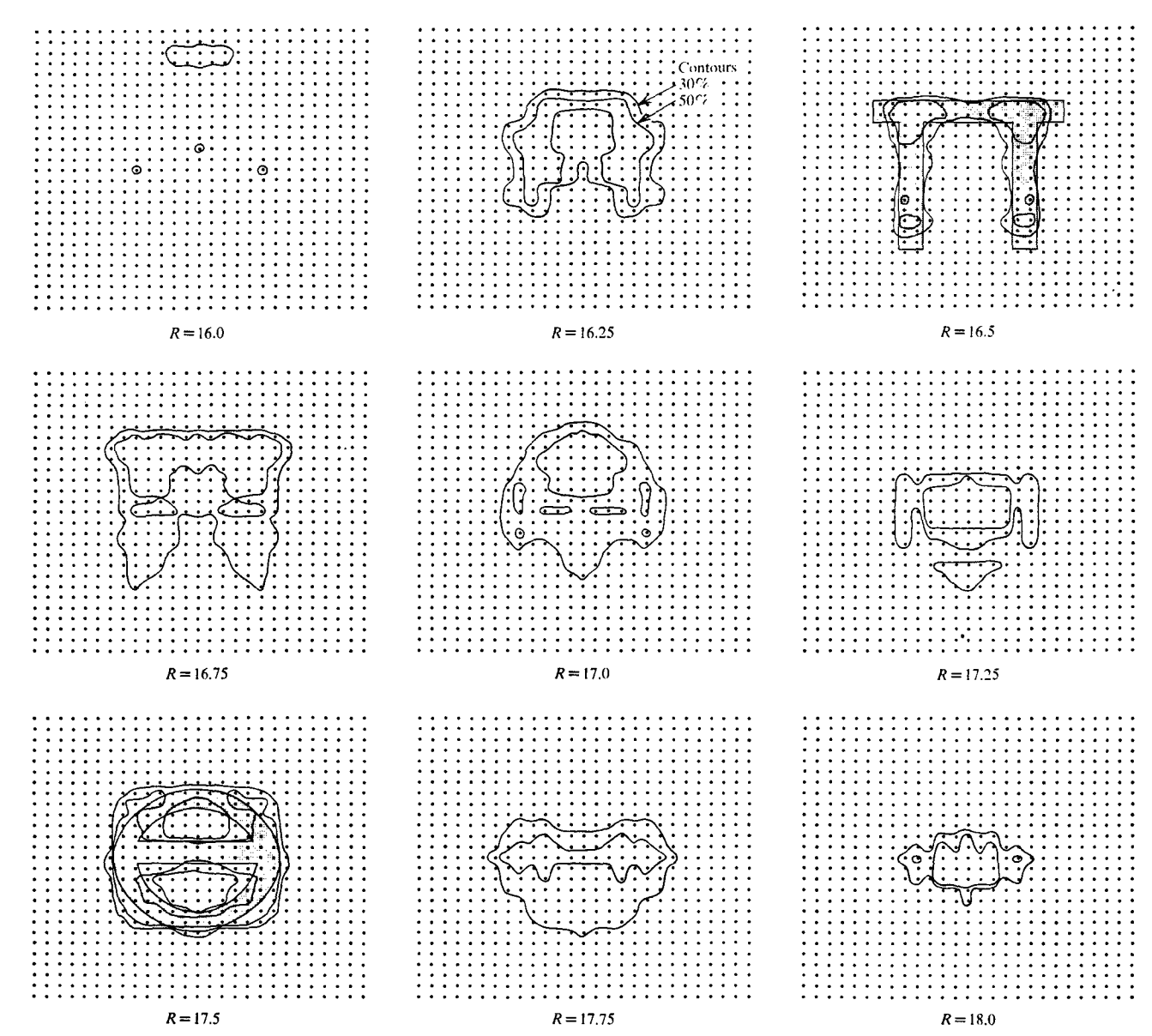


Figure 10 A single pulse hologram yielded these image reconstructions on the spherical surfaces R = 16.0 to R = 18.0. The 30% and 50% contours are determined with respect to the maximum intensity of each of the reconstructions. The maximum intensities, given as fractions of the maximum intensity at R = 16.5, are 0.029, 0.28, 1.00, 0.45, 0.22, 0.57, 0.74, 0.60 and 0.20, from R = 16.0 to 18.0, respectively.

range, each corresponding to one-half the nominal resolution distance.

Figure 10 is the reconstruction corresponding to the image in Fig. 9(a). The figures  $\Pi$  and  $\theta$  are clearly discernable, even through they are separated in range by only a distance  $\lambda$ . The hologram from which these images are reconstructed has been generated on the assumption that the figures are weak scatterers, so that the  $\Pi$  does not obstruct the return from the  $\theta$  directly behind it. The images have been individually normalized to save computer storage, so that the 30% and 50% contours are not directly comparable among different images. For

example, the irregular figure appearing at R=17.0, half-way between the  $\Pi$  and the  $\Theta$ , reaches a maximum intensity of only 22% of the maximum  $\Pi$ -intensity. In a three-dimensional intensity plot, the  $\Pi$  and  $\Theta$  would stand out clearly.

The hologram of a weakly scattering hemisphere is shown in Fig. 11. Diffraction "ringing" from the curved reflecting surface is evident in the several phase reversals. Statistical averaging over many reflecting points has suppressed the anomalies due to rectangular digital quantization, except at the small amplitudes, and the zones are properly curvilinear.

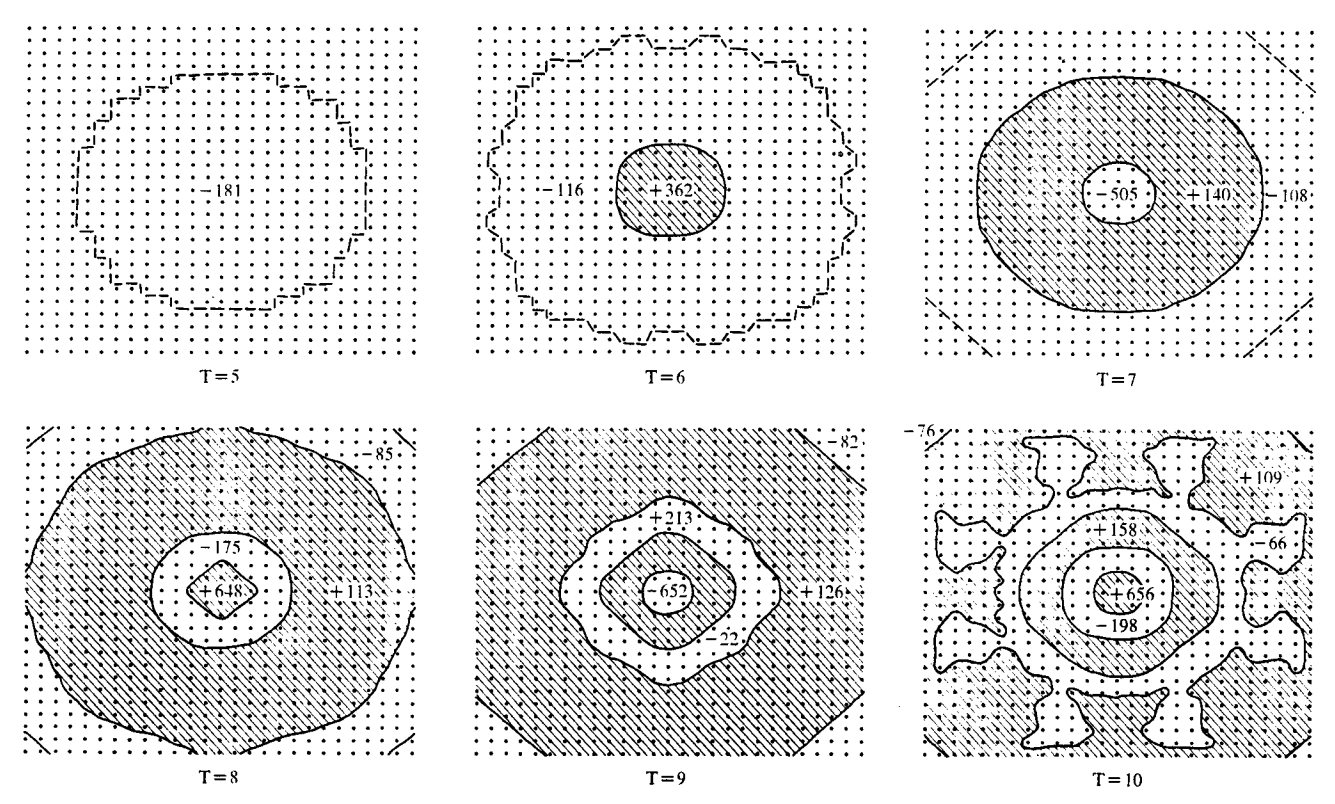


Figure 11 Pulse hologram of hemisphere for times between first echo arrival at T = 5 and T = 10. Crosshatching represents zones of positive amplitude and the inscribed numbers denote peak amplitudes within each zone.

The corresponding reconstruction, Fig. 12, spans R=15.0 to R=18.5. The pole of the hemisphere is at R=15.5. The 50% contours genuinely outline the reflecting surface—a fact more convincingly evident in three dimensions with a set of stacked transparencies. Crossed-array geometry and digital quantization combine to cause some rectangular distortion, particularly between R=15.0 and 16.25. Notice the "animal pelt" at R=16.0. The specular highlight at the hemisphere pole is noticeable only as a moderately increased intensity beginning one range increment (0.25) in front of the actual pole. The anomalous decrease of the contour size at R=16.0 is probably due to coherent interference from the polar highlight.

The reconstructions exhibited above comprise  $27 \times 27 \times 16$  three-dimensional image points, i.e., about 12,000. Reconstructions via Eq. (4) for renditions of this degree of detail require roughly  $10^7$  elementary computations, a task well within the capacity of a moderate-sized computer. As soon as actual pulsed acoustic holograms are available in place of simulations, these computer reconstruction techniques will yield images of hitherto unobtainable three-dimensional fidelity.

#### References

- 1. Willard H. Wells, "Acoustic Imaging with Linear Transducer Arrays," Acoustical Holography, Volume 2, edited by A. Metherell and Lewis Larmore, Plenum Press, New York, 1970.
- K. Preston, Jr. and J. L. Kreuzer, "Ultrasonic Imaging Using a Synthetic Holographic Technique," Appl. Phys. Letters 10, 5 (1967).
- A. Metherell and S. Spinak, "Acoustic Holography of Non-existent Wavefronts Detected at a Single Point in Space," Appl. Phys. Letters 13, 22 (1968).
- J. W. Goodman and R. W. Lawrence, "Digital Image Formation from Electronically Detected Holograms," Appl. Phys. Letters 11, 3 (August 1, 1967).
- R. A. Peterson, "Seismography 1970, The Writing of Earth Waves," a paper presented at the Symposium on Seismic Waves from Vibrational Sources, the Pacific Coast Section of the Society of Exploration Geophysicists, November 14, 1969.
- A. Fontanel and G. Grau, "Applications of Impulse Seismic Holography," a paper presented at the 39th Annual Meeting of the Society of Exploration Geophysicists, Calgary, Canada, September 1969.
- J. W. Goodman, Introduction to Fourier Optics, Mc-Graw-Hill Book Company, Inc., New York, 1968, pp. 45-46.

Received January 12, 1970

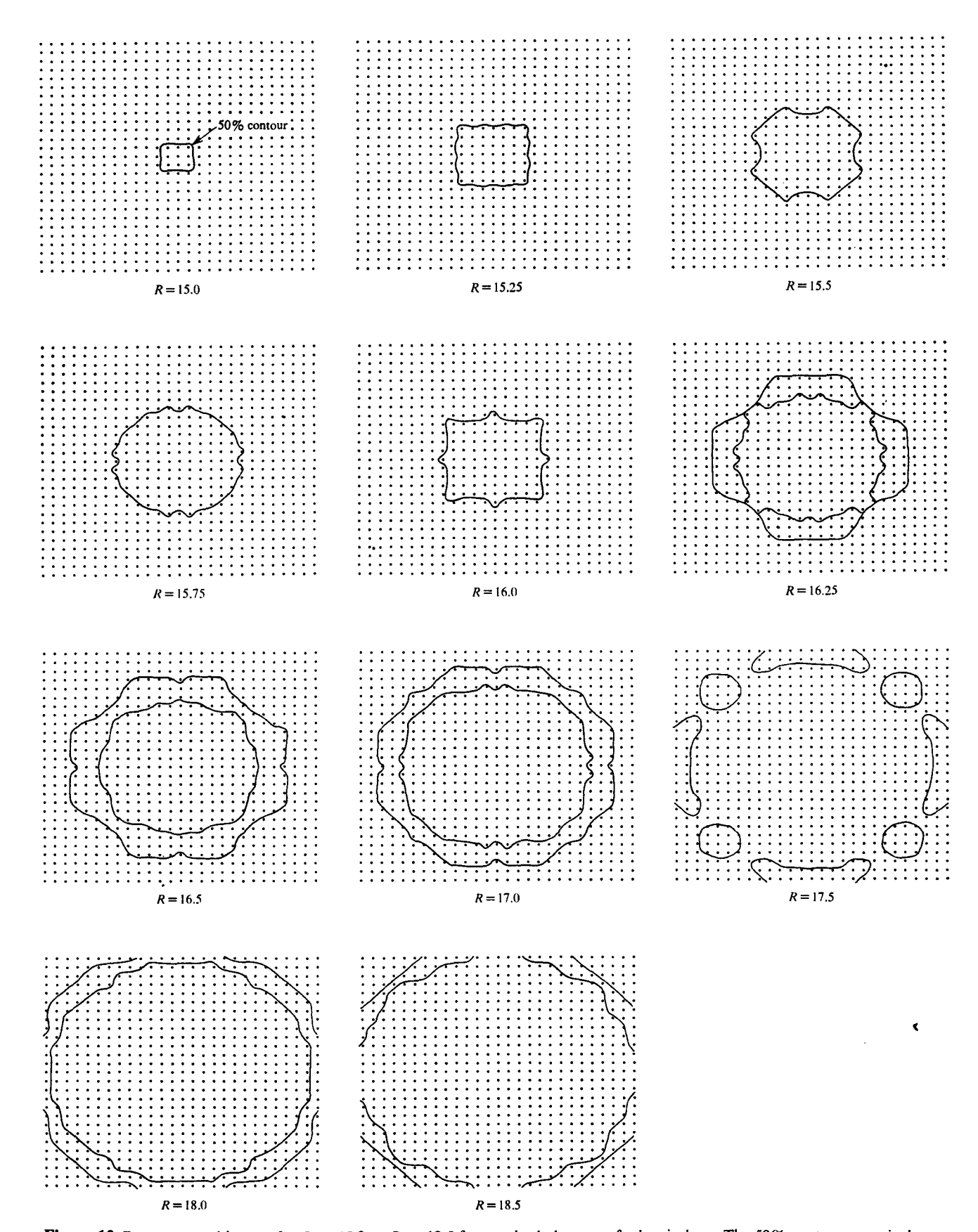


Figure 12 Reconstructed images for R = 15.0 to R = 18.5 from pulse hologram of a hemisphere. The 50% contours genuinely outline the reflecting surface. Rectangular distortion is evident, particularly at ranges less than R = 16.5.